Chemical Engineering Journal 166 (2011) 105–115

Contents lists available at ScienceDirect

Chemical Engineering Journal

journal homepage: www.elsevier.com/locate/cej

A mathematical model for non-monotonic deposition profiles in deep bed filtration systems

Hao Yuan*, Alexander A. Shapiro

Department of Chemical and Biochemical Engineering, Technical University of Denmark, DTU Building 229, 2800 Lyngby, Denmark

ARTICLE INFO

Article history:
Received 14 July 2010
Received in revised form 13 October 2010
Accepted 14 October 2010

Keywords:
Suspension
Colloid
Porous media
Surface associated phase
Non-monotonic deposition

ABSTRACT

A mathematical model for suspension/colloid flow in porous media and non-monotonic deposition is proposed. It accounts for the migration of particles associated with the pore walls via the second energy minimum (surface associated phase). The surface associated phase migration is characterized by advection and diffusion/dispersion. The proposed model is able to produce a non-monotonic deposition profile. A set of methods for estimating the modeling parameters is provided in the case of minimal particle release. The estimation can be easily performed with available experimental information. The numerical modeling results highly agree with the experimental observations, which proves the ability of the model to catch a non-monotonic deposition profile in practice. An additional equation describing a mobile population behaving differently from the injected population seems to be a sufficient condition for producing non-monotonic deposition profiles. The described physics by the additional equation may be different in different experimental settings.

1. Introduction

Modeling suspension or colloid flow in porous media is of great importance to a large variety of applications, e.g. deep bed filtration, membrane filtration, drilling mud filtration, bacteria and viruses spreading in underground water and others [1,2]. A considerable effort is going on aimed at understanding the transport and deposition of suspended particles in porous media. Especially, non-Fickian transport and non-exponential deposition of the particles, such as hyperexponential and non-monotonic deposition profiles attract significant interest [3–8].

The conventional methodology, ADE with a single filtration coefficient, only predicts exponentially decreasing deposition profiles [3]. Many of the experimental results, on the other hand, show hyperexponential deposition profiles or even non-monotonic deposition profiles under some specific conditions [9–13]. Most of these experiments are carried out in the presence of an energy barrier, for example similarly charged colloid particles and median particles. The deposition of colloids is theoretically hindered by the repulsion between the colloid and porous media. The mechanisms of the deposition in such cases are likely to encompass enhanced retention at low-velocity zones of pore space, staining at grain–grain contacts, surface charge heterogeneity, deposition in the second energy minimum, and surface roughness [4,8,11,14–19]. Both pore structure and velocity are observed to have impacts on the deposition profiles [18,20].

Colloids carried by the flowing fluid may be captured at single-contacts of porous media via the second energy minimum or the primary energy minimum [10,11,14,21]. Deposition of colloids may also occur at grain–grain contacts (pore constrictions, stagnant zones) via straining [9,18,20,22–24]. The balance between the hydrodynamic torque from the flowing fluid and the resisting adhesive torque determines whether the colloids adjacent/attached to the pore walls will be immobilized or re-entrained into the carrying fluid [8,19,25–29].

Under unfavorable attachment conditions where the DLVO calculations can preclude most of single-contact deposition via the primary energy minimum, the captured particles via the second energy minimum are subject to the hydrodynamic drag and down-gradient translation [8,10,16,19,30–32]. Close to the grain–grain contacts some of the surface-associated particles may be immobilized in the stagnant zones. Others are entrained by the flowing fluid and may either rejoin the bulk phase or jump to the next grain [16,18,20,23,24,29,33].

The commonly reported hyperexponential deposition has been attributed to the heterogeneity of the surface charge and energy minima [11,12,34,35] or to the enhanced retention at low-velocity zones of pore space [17,22,23]. Based on the described mechanisms, the authors developed various models which produce hyperexponential deposition. In Refs. [11,12,35,36], distribution of filtration coefficients was applied to reflect the heterogeneity of particle population and particle-pore interactions. In Refs. [17,37], dual-

* Corresponding author. Tel.: +45 45252864.
E-mail address: hy@kt.dtu.dk (H. Yuan).

1385-8947/$ – see front matter © 2010 Elsevier B.V. All rights reserved.
doi:10.1016/j.cej.2010.10.036

Nomenclature

c	number of suspended particles per unit pore volume (m^{-3})
C	dimensionless suspended particle concentration
s	number of retained particles per unit pore volume (m^{-3})
s	dimensionless retained particle concentration
s_m	number of particles in the surface associated phase per unit pore volume (m^{-3})
S_m	dimensionless particle concentration in the surface associated phase
t	time (s)
T	dimensionless time (pore volume)
t_0	particle injection duration (s)
T_0	dimensionless particle injection duration (pore volume)
x	x coordinate in space
X	dimensionless x
v	advection velocity of particles in the bulk aqueous phase
v_m	advection velocity of particles in the surface associated phase
u	dimensionless advection velocity of particles in the bulk aqueous phase
u_m	dimensionless advection velocity of particles in the surface associated phase
D	coefficient of dispersion (m^2/s) in the bulk aqueous phase
D_m	coefficient of diffusion (m^2/s) in the surface associated phase
R	dimensionless longitudinal dispersivity in the bulk aqueous phase
R_m	dimensionless longitudinal diffusivity in the surface associated phase
c_0	influent concentration
f_m	ratio of v_m to v
$d_{\max}$	maximum diameter of a pore
d_{media}	diameter of the median particle
$d_{colloid}$	diameter of the colloid particle
d_c	constriction diameter
d_z	pore diameter in position z
h	pore length
$v_{colloid}$	fluid velocity at the center of the particle associated with the pore wall
$D_{effective}$	effective diameter of pores
N_{pore}	number of pores in a cross-section of the column
λ_s	coefficient of particle transport from the bulk aqueous phase to the surface associated phase (s^{-1})
Λ_s	dimensionless form of λ_s
λ_d	coefficient of particle transport from the bulk (flowing) phase to the immobilized phase (s^{-1})
Λ_d	dimensionless form of λ_d
λ_m	coefficient of particle transport from the surface associated phase to the deposition phase (s^{-1})
Λ_m	dimensionless form of λ_m
λ_{mr}	coefficient of particle transport from the surface associated phase to the bulk phase (s^{-1})
Λ_{mr}	dimensionless form of λ_{mr}
λ_r	coefficient of particle transport from the immobilized phase to the bulk phase (s^{-1})
Λ_r	dimensionless form of λ_r
λ_{ar}	coefficient of particle transport from the deposited aggregates to the flowing aggregates (s^{-1})
Λ_{ar}	dimensionless form of λ_{ar}
λ_{ad}	coefficient of particle transport from the flowing aggregates to deposition (s^{-1})
Λ_{ad}	dimensionless form of λ_{ad}
φ	porosity of the column/porous medium
C_s	average dimensionless effluent concentration at the steady stage

permeability models were developed to take into account the high-velocity zones and low-velocity zones of pore space.

On the other hand, the observed non-monotonic deposition has been attributed to the lagged release of aggregates at straining sites [18], or to the migration of surface associated colloids via the second energy minimum [16]. In the same respective works the authors developed conceptual models based on the mechanisms. Both models considered a third phase flowing in porous media. In Ref. [18], Bradford, Simunek, and Walker described the released aggregates transporting and depositing at different rates from the monodisperse colloids. This model will further be referred to as the BSW model. In Ref. [16] the authors proposed that migration of the surface associated phase should accompany the bulk flow.

The model parameters in Ref. [18] were estimated by fitting the model to experiments. This model was shown to be able to simulate non-monotonic deposition profiles. On the contrary, the model in Ref. [16] was proposed only on the conceptual level. Transport and interactions of the migratory surface phase and the bulk aqueous phase were not assigned with detailed physical and mathematical descriptions. Whether the model considering the surface flow can be used to simulate deep bed filtration processes remained unknown.

The purpose of this paper is to establish a model for deep bed filtration considering the migration of the surface associated phase [16]. We end up with the model that is simpler and contains less adjustment parameters than the BSW model, but still can simulate pretty precisely non-monotonic deposition profiles. The effects of the different migration properties (migration velocity, deposition rates, etc.) are studied. The modeling results are also compared to the experiments where non-monotonic deposition profiles are observed. The proposed model is compared to the BSW model to investigate the mathematical condition for deposition non-monotonicity.

2. Model establishment

2.1. Basic assumptions

Under unfavorable attachment conditions, the DLVO calculations may preclude most of single-contact deposition via the primary energy minimum. The torque balance calculations may indicate that the captured particles via the second energy minimum are subject to the hydrodynamic drag and down-gradient translation [8,10,16,19,30–32]. Under such specific conditions, we may follow Li et al. [16] to assume that the particles captured by porous media can be classified into two phases, the migratory surface associated phase (weak association via second energy minima at single-contacts) and the immobilized phase (retention via straining at grain–grain contacts), as seen in Fig. 1.

It is assumed that the transport of the monodisperse particles in the bulk aqueous phase can be characterized by an advection–dispersion equation with a single sink term and a source term. The sink term represents the transport of particles from the bulk phase to the migratory SA phase and to the immobilized phase while the source term represents the mass transfer from the SA phase and the immobilized phase to the bulk phase.

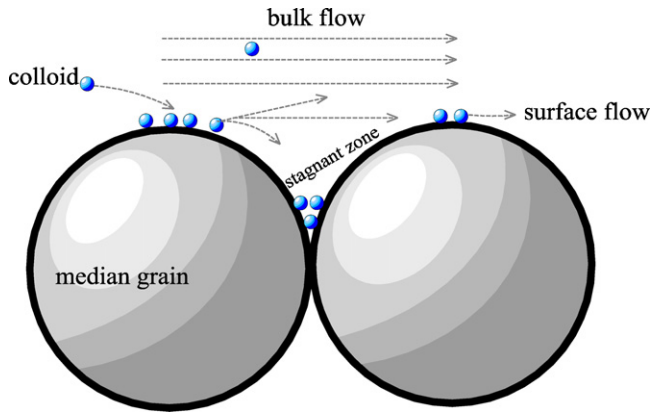

Fig. 1. Illustration of the surface associated phase and the bulk aqueous phase at pore scale.

It is assumed that the migration of the SA phase can be described by the common advection–diffusion formalism. The column inlet is usually connected to an open source of colloids without porous media, hence the zero SA phase is set as the inlet boundary condition. The SA phase may migrate from one grain to another in the following sense: Some of the colloids close to grain–grain contacts are entrained by the flowing fluid and may either rejoin the bulk phase or jump to the next grain. Others may be immobilized in the stagnant zone around grain–grain contacts.

A convective diffusion mechanism of the SA phase may be assumed. A dispersion length is usually interpreted as a characteristic scale of heterogeneity of the porous medium. The dispersion lengths in the bulk phase and the SA phase may, generally speaking, be different, since the surface may be more tortuous than the pore space. However, the orders of magnitude of these parameters in the not-so-highly heterogeneous porous media may be the same. For simplicity of the model and minimization of the number of adjustment parameters, we assume the two dispersion lengths to be equal. This assumption will be validated by comparison with experimental data.

The case of a dilute suspension is considered. The volume of the SA phase and that of the retained particles are assumed to be minimal compared to the bulk aqueous phase, so that their existence does not affect the pore structure significantly. The porosity is assumed to be constant during the entire filtration process. The particle concentration in the SA phase, on the other hand, may be comparable to that in the bulk aqueous phase.

One-dimensional flow is considered, since it is common to most of the experiments and for many applications. The theory is readily generalized onto multiple dimensions.

2.2. System of equations

The system of equations following from the above assumptions has the form of:

$$\frac{\partial c}{\partial t} + v\frac{\partial c}{\partial x} = D\frac{\partial^2 c}{\partial x^2} + (\lambda_r s + \lambda_{mr} s_m) - (\lambda_s + \lambda_d)c, \tag{1}$$

$$\frac{\partial s_m}{\partial t} + v_m\frac{\partial s_m}{\partial x} = D_m\frac{\partial^2 s_m}{\partial x^2} + \lambda_s c - (\lambda_m + \lambda_{mr})s_m, \tag{2}$$

$$\frac{\partial s}{\partial t} = \lambda_m s_m + \lambda_d c - \lambda_r s. \tag{3}$$

Here c is the number of particles in the bulk aqueous phase per unit pore volume, v is the velocity of the particles in the bulk aqueous phase, and D is the dispersion coefficient in the bulk aqueous phase. Subscript 'm' represents the 'migratory surface associated phase' and s_m is the number of particles in the SA phase per unit pore volume. Correspondingly, v_m is the advection velocity of the particles in the SA phase and D_m is the diffusion coefficient in the SA phase. Finally, s is the concentration of the immobilized particles. $\lambda_s c$ in Eqs. (1) and (2) represents the particle transport from the bulk aqueous phase to the SA phase, $\lambda_d c$ in Eq. (1) is the transport directly from the bulk aqueous phase to the immobilized deposition, and $\lambda_m c$ in Eq. (2) represents the conversion from SA phase into the immobilized deposition. $\lambda_r s$ represents the release of immobilized particles while $\lambda_{mr} s_m$ represents the release of SA phase back to the bulk phase. In order to connect the motion of the particles in the SA phase to that in the bulk aqueous phase, the following relation is adopted:

$$v_m = f_m v, \tag{4}$$

where f_m is the ratio of the particle velocity in the SA phase to that in the bulk aqueous phase. The estimation of the fraction will be discussed in detail later. Convective dispersion/diffusion both in the bulk aqueous phase and the surface associated phase is also assumed:

$$D = \alpha v; \quad D_m = f_m D, \tag{5}$$

where α is the longitudinal dispersivity/diffusivity possessing the dimension of length, the same both in the bulk aqueous phase and in the SA phase.

Unlike most common formulations, system (1)–(3) does not involve porosity of the medium, and the deposition and release rates are not proportional to velocity. This is a possible formulation for the case of constant porosity (dilute suspension), if we assume that v and v_m are constant and interstitial, but not superficial, flow velocities and give corresponding re-definitions of the filtration coefficients $\lambda_s, \lambda_d, \lambda_m, \lambda_r, \lambda_{mr}$. These re-definitions should be taken into account when actual values of the coefficients are computed.

Similar to [36,38], the system of Eqs. (1)–(3) can be reformulated in terms of dimensionless variables:

$$\frac{\partial C}{\partial T} + u\frac{\partial C}{\partial X} = uR\frac{\partial^2 C}{\partial X^2} + (\Lambda_r S + \Lambda_{mr} S_m) - (\Lambda_s + \Lambda_d)C, \tag{6}$$

$$\frac{\partial S_m}{\partial T} + u_m\frac{\partial S_m}{\partial X} = u_m R_m\frac{\partial^2 S_m}{\partial X^2} + \Lambda_s C - (\Lambda_m + \Lambda_{mr})S_m, \tag{7}$$

$$\frac{\partial S}{\partial T} = \Lambda_m S_m + \Lambda_d C - \Lambda_r S. \tag{8}$$

Here $x = LX$, $t = (L/v_0)T$, $c = Cc_0$, $s_m = S_m c_0$, $v_m = u_m v_0$, $R_m = D_m/v_0 L$, $\Lambda_m = \lambda_m L/v_0$, $s = Sc_0$, $v = uv_0$, $R = D/v_0 L$, $\Lambda_s = \lambda_s L/v_0$, $\Lambda_d = \lambda_d L/v_0$, $\Lambda_{mr} = \lambda_{mr} L/v_0$, and $\Lambda_r = \lambda_r L/v_0$.where R is the dimensionless longitudinal dispersivity in the bulk aqueous phase and R_m is the dimensionless longitudinal diffusivity in the SA phase. The value of L is the reference length (m), v_0 is the reference velocity (m/s), and c_0 is the reference concentration. The inverse Peclet number R describes the magnitude of the spatial dispersion compared to the product of the reference velocity and the reference length, while R_m is a similar value for the surface phase. Provided that v_0 is the particle velocity in the bulk phase ($v = v_0$) and that the longitudinal dispersivities/diffusivities in the bulk phase and in the SA phase are equal, the dimensionless parameters can be expressed as:

$$u = 1, \quad u_m = f_m, \quad R_m = R. \tag{9}$$

Eqs. (6)–(8) represent mass balances of the particles in the bulk, surface, and immobile phase, correspondingly. With given velocities and dispersion/diffusion coefficients, the three equations form a closed system for the entire mass balance among the bulk aqueous phase, the SA phase and the immobilized deposition phase.

A simpler formulation has also been tested: a system where deposition from the bulk to the immobile phase is prohibited, $\Lambda_d = 0$. Sample calculations (not shown here) indicated that with such a formulation the deposition at the inlet is zero because the

SA phase concentration is assumed to be zero at the inlet. Indeed, all the particles deposited at the inlet belong to the SA phase and immediately start moving forward along the sample. This is in contradiction with the observed deposition profiles [4,16,18] with non-zero deposition near the entrance. Therefore, deposition from the bulk directly to the immobile phase should be introduced to avoid discrepancy with the observed experimental data.

Summing Eqs. (6)–(8) together leads to the mass conservation law:

$$\frac{\partial(C+S+S_m)}{\partial T}+u\frac{\partial(C-R(\partial C/\partial X)+f_mS_m-f_mR_m(\partial S_m/\partial X))}{\partial X}=0. \tag{10}$$

Eq. (10) indicates that the boundary conditions at the inlet $X=0$ should take into account both the advection flux and the dispersion/diffusion flux of the particles.

2.3. Boundary conditions

Clean bed filtration is assumed as the initial condition for the convenience of comparing modeling results with the column experiments in most labs. The initial conditions can be formulated as:

$$C(X,T=0)=0;\quad S_m(X,T=0)=0;\quad S(X,T=0)=0. \tag{11}$$

Since Eqs. (6) and (7) are both parabolic, it is commonly accepted to apply Neumann boundary conditions at the outlet and two Robin boundary conditions at the inlet for the mobile phases [39]:

$$C-R\frac{\partial C}{\partial X}=\begin{cases}1 & (X=0,T<T_0)\\ 0 & (X=0,T\geq T_0)\end{cases}, \tag{12}$$

$$\left.\frac{\partial C}{\partial X}\right|_{X=L}=0, \tag{13}$$

$$S_m-R_m\frac{\partial S_m}{\partial X}=0\quad(X=0,T), \tag{14}$$

$$\left.\frac{\partial S_m}{\partial X}\right|_{X=L}=0. \tag{15}$$

Boundary condition (12) represents the common injection procedure: before T_0, inject particles, and after T_0, inject pure water. The ad hoc boundary condition (14) is based on the assumption that inlet of the porous medium is usually connected with a source domain without porous media. Thus, no surface associated phase is formed directly at the inlet. Formation of the surface phase does not begin until at the inlet, and any such phase moves further by the surface flux. Of course, in case of an immobile surface phase alone, Eq. (14) is violated. Neumann boundary conditions (13) and (15) represent the no-flux setting at the outlet of an experimental column.

Addition of Eqs. (12)–(14) and addition of Eqs. (13)–(15) lead to the total boundary conditions for both mobile phases indicated by Eq. (10):

$$C-R\frac{\partial C}{\partial X}+S_m-R_m\frac{\partial S_m}{\partial X}=\begin{cases}1 & (X=0,T<T_0)\\ 0 & (X=0,T\geq T_0)\end{cases}, \tag{16}$$

$$\left.\frac{\partial C}{\partial X}+\frac{\partial S_m}{\partial X}\right|_{X=L}=0. \tag{17}$$

2.4. Implementation

It is assumed that the velocities, dispersivity and diffusivity, as well as the coefficients of particle transport to different phases are all constant and known. The closed system of Eqs. (6)–(8), with boundary conditions (11)–(14), can easily be solved by a finite difference technique. The calculation is implemented in MATLAB with the intrinsic function 'pdepe' for solving partial differential equations and 'ode15s' for solving ordinary differential equations. The numerical solution with $\Lambda_s=0$ (no SA phase) is also compared with the analytical solution in Ref. [39]. The error of the numerical solution can be reduced to 0.01% with a properly selected mesh. An approximate analytical solution for the model can also be found in Ref. [39]. A good agreement between the analytical solution and numerical solution is observed (not shown here). This validates the selected numerical method.

In order to reveal the modeling results in the same way as those from the laboratory experiments, the total effluent concentration and the total deposition need to be calculated. The bulk aqueous phase and the SA phase move at two different velocities in parallel. Since the experimentally monitored effluent concentration counts both the number of particles in the bulk aqueous phase and that in the SA phase per unit time, the total effluent concentration can be calculated by:

$$C_{effluent}(T)=\frac{uC(1,T)+u_mS_m(1,T)}{u}=C(1,T)+f_mS_m(1,T). \tag{18}$$

At the end of a column experiment ($T=T_{\max}$), the flow in the core is zero and the SA phase remains immobile. The final deposition is then the sum of remaining SA phase and the immobilized phase:

$$S_{final}(X)=S(X,T_{\max})+S_m(X,T_{\max}). \tag{19}$$

The model parameters may be estimated by fitting the modeling results to the experimental data. The MATLAB intrinsic function 'lsqnonlin' for non-linear least square problems is applied for curve fitting. Confidence intervals (CI) and correlation matrices of the model parameters are calculated. Details of the procedure can found in Refs. [40,41].

2.5. Magnitude of the SA phase migration

Ratio f_m of the velocities in the surface phases and in the bulk is a crucial parameter to describe the migration of the SA phase. Although a priori estimation of the exact value of f_m is problematic, its magnitude may be found on the basis of simple considerations. In Appendix, we show this evaluation, as previously discussed in [26,42].

These considerations are approximate. They are based on the assumption that the average velocity of SA phase is of the same magnitude as the fluid velocity close to the solid surface. Pore scale simulations show however that the fluid velocity close to the solid surface may vary by several orders of magnitude even in homogeneous porous media [26,43–46]. Roughness may also contribute to the value of f_m.

3. Results of modeling

This section aims at studying the basic properties of the proposed model and the effects resulting from changing the properties of the SA phase migration, such as the advection velocity, the diffusivity and the deposition rate of the SA phase.

3.1. Numerical solutions

Numerical solutions are first obtained with all the parameters assumed to be constant and known. Particles are injected in the first five pore volumes, and then water alone is injected to wash away the remaining mobile particles until fifteen pore volumes are injected. For the calculations we use: $R=6.67\times10^{-3}$; $u=1.0$;

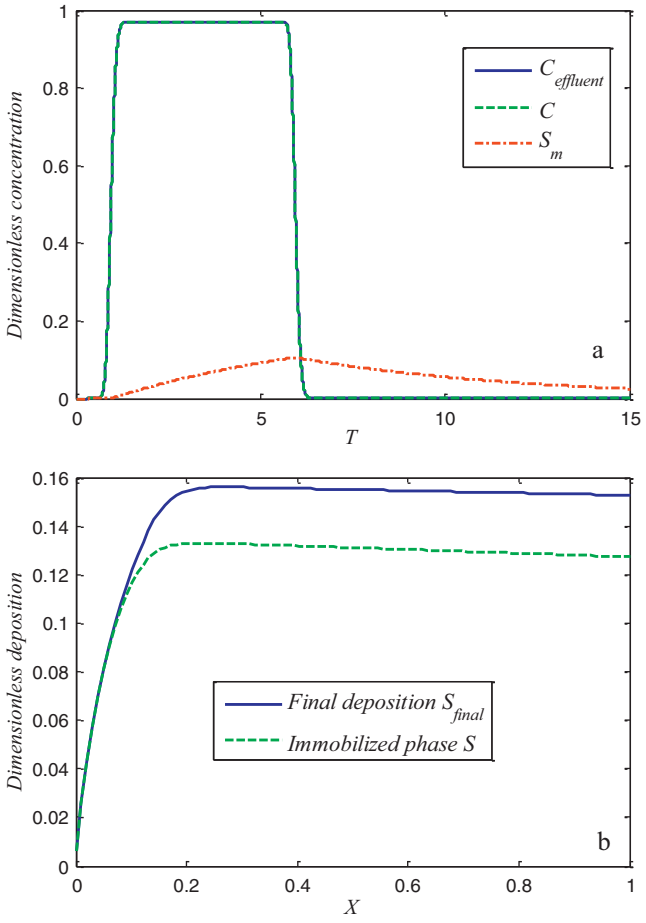

Fig. 2. (a) Concentrations at the outlet and (b) final deposition and immobilized phase at the end of flooding.

$\Lambda_s = 0.03$; $\Lambda_d = 0.012$; $f_m = 0.01$; $\Lambda_m = 0.15$; $\Lambda_{mr} = 0.15 \times 10^{-3}$; $\Lambda_r = 0$. The calculated profiles are shown in Figs. 2–4.

As seen in Fig. 2(a), the particle concentration in the SA phase at the outlet is comparable to that in the bulk aqueous phase.

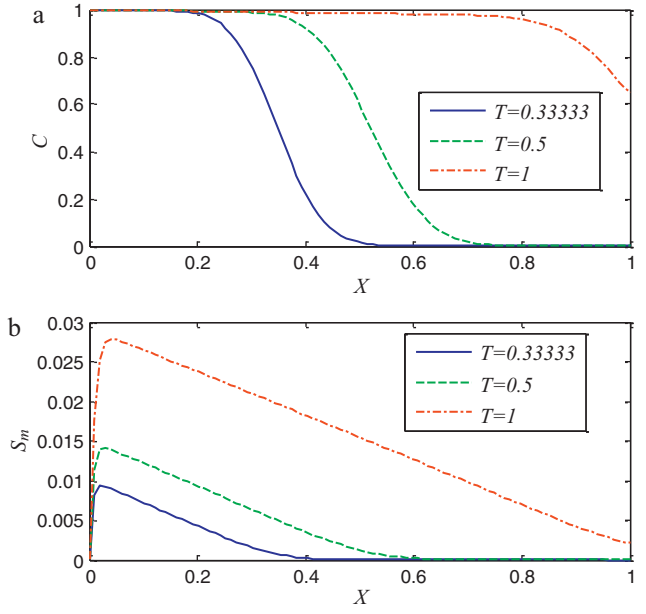

Fig. 3. Displacement profiles: (a) bulk aqueous phase, (b) surface associated phase.

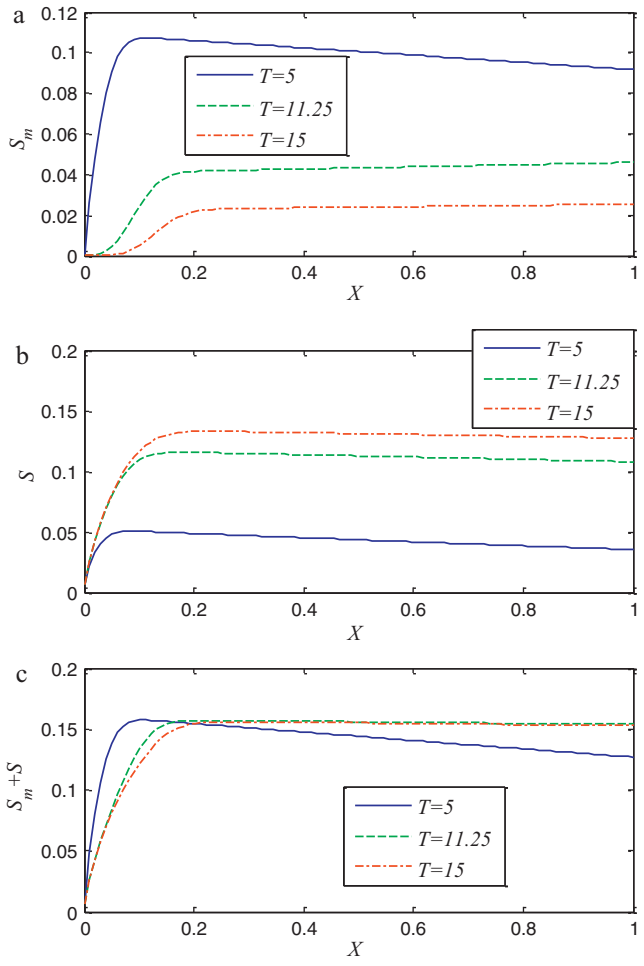

Fig. 4. (a) Surface associated phase, (b) immobilized phase, and (c) total deposition.

However, the major contribution to the monitored effluent concentration is from the bulk aqueous phase alone. It is explained by the far slower motion of the SA phase than that of the bulk aqueous phase. Fig. 2(b) reveals the non-monotonic spatial distribution of the immobilized particles and that of the final deposition. The difference between them indicates that the immobilization of the SA phase due to ceased flooding contributes to the final deposition. It proves that the mechanism of migratory surface phase alone can give rise to a non-monotonic deposition profile.

Fig. 3(a) and (b) shows the displacement fronts of the bulk phase and the SA phase, respectively at different time moments before breakthrough. It can be seen that the front of the SA phase lags behind that of the bulk phase. The distribution of the SA phase is strongly non-monotonic and possesses a peak moving towards the outlet. Fig. 4 shows the evolution of immobilized particles with the SA phase and the resulting total deposition. Before the end of injection ($T < 5$) the SA phase accumulates and is non-monotonic along X, while the peak of the SA phase is flushed to the outlet during water flooding ($T > 5$). The resulting immobilized phase is distributed non-monotonically over the entire process, and its peak moves towards the outlet. It can be inferred from the results that the final deposition is still non-monotonic in the case of no immobilized phase, because the SA phase itself is non-monotonically distributed along X.

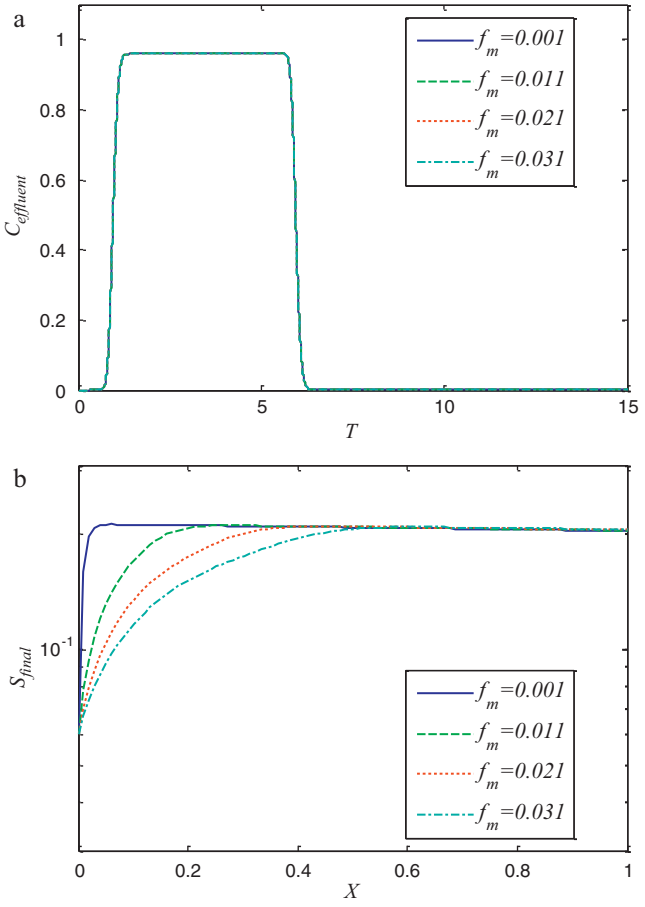

Fig. 5. Comparison of different values of f_m.

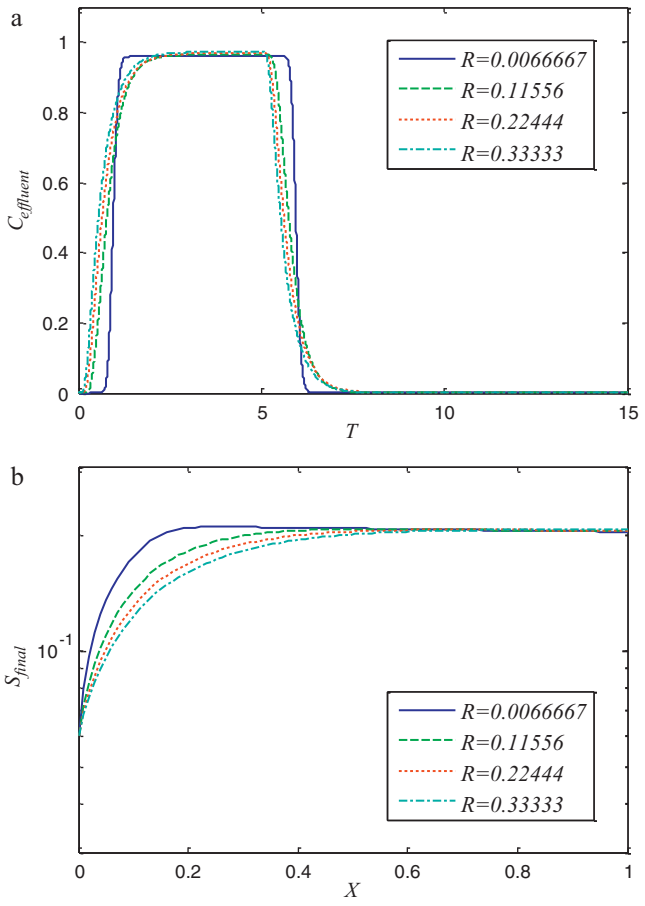

Fig. 6. Comparison of different values of R.

3.2. Migration of surface associated phase

Calculations are then carried out with different values of f_m. The rest of the parameters are set to the same as in Section 3.1. As seen in Fig. 5(b), the larger f_m leads to maximum final deposition closer to the inlet. The faster the SA phase migrates the closer the maximum of deposition is to the outlet. On the other hand, since the effluent SA phase contributes little to the total effluent concentration, the breakthrough curve is not much influenced by this factor.

The modeling results may also enlighten some aspects in the experimental design for observing non-monotonic deposition. Since larger values of f_m help non-monotonicity of deposition, larger colloids and smaller median particles are preferable for such experiments. Other aspects, such as the optimal solution chemistry and particle materials, are beyond the scope this work.

3.3. Dispersivity

Calculations are carried out with varying dispersivity R. The chosen value for f_m is 0.01, and the rest of the parameters are the same as in Section 3.1. It is shown in Fig. 6(b) that larger values of R also lead to the peak of final deposition closer to the outlet. This behavior, however, is also connected with transport of the bulk aqueous phase, as seen in Fig. 6(a). As expected, larger values of dispersivity result in a larger wash-out of the breakthrough curve.

3.4. Generation of SA phase

Calculations are carried out with various SA phase generation rate coefficients Λ_s. The rest of the parameters are the same as in Section 3.1. Since at the end of flooding the remaining SA phase in the system also stops flowing, it contributes to the final deposition. The expected effect is confirmed in Fig. 7(b). It also shows that the large value of Λ_s leads to maximum deposition slightly closer to the outlet. This can be explained by the fact that the faster SA phase generation gives rise to more SA phase available for migration per unit time. Compared to the classical filtration theory, Λ_s is a part of the total filtration coefficient. Hence, the larger value to Λ_s leads to the lower effluent concentration at the steady stage, as seen in Fig. 7(a).

3.5. Immobilization of SA phase

Calculations are carried out with various SA phase immobilization rate coefficients Λ_m. The rest of the parameters are the same as in Section 3.1. Fig. 8(b) shows that the faster deposition of SA phase leads to maximum deposition closer to the inlet. The result corresponds to that in Fig. 7(b). In a similar sense, the faster deposition of the SA phase gives rise to less SA phase available for migration in a unit time. In other words, a particle in the SA phase may not have enough time to migrate farther before it is deposited. Again the factor has little influence on the breakthrough curve, as seen in Fig. 8(a).

4. Comparisons with experiments

In this section, the modeling results are compared to the experimental observations. Model parameters are estimated either by fitting the model to experimental data or by a proposed estimation method. The purpose is to find a fast method for estimating

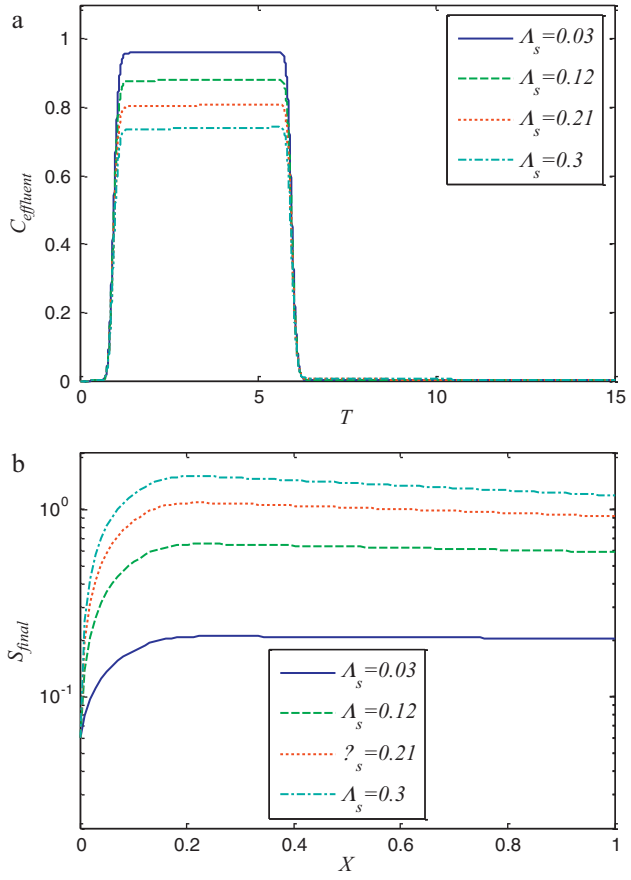

Fig. 7. Comparison of different values of Λ_s.

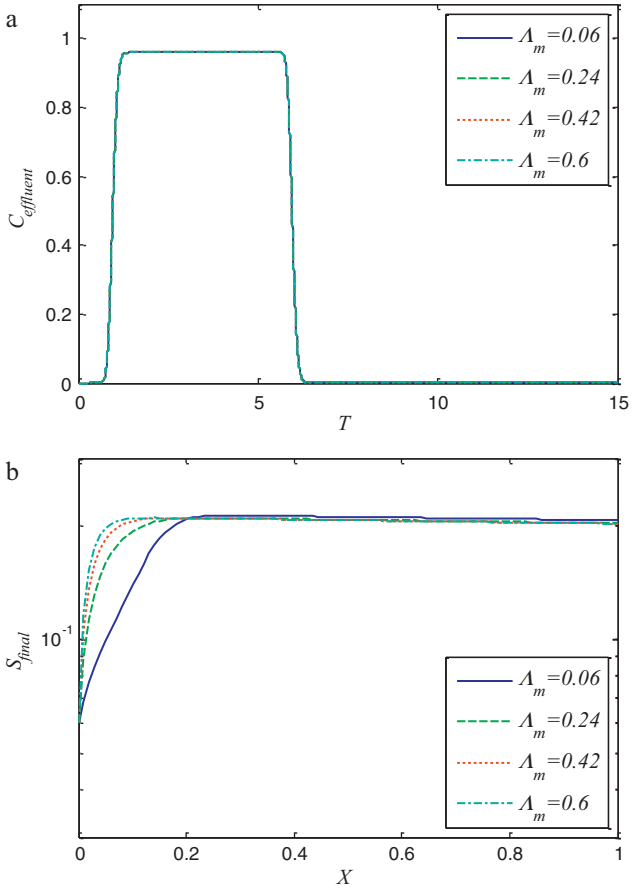

Fig. 8. Comparison of different values of Λ_m.

the parameters of the model, and to match the modeling and the experimental results, by applying the knowledge obtained from the numerical modeling above.

Li and Johnson [4] adopted the fluorescent carboxylate-modified polystyrene latex microspheres (diameter 1.1 μm) as colloid particles and packed quartz sand (diameter 417–600 μm) as porous media for the column experiments. Non-monotonic deposition profiles were observed in the experiments.

First, the parameters are estimated by fitting the model to the breakthrough curves and the deposition profiles from Ref. [4]. The parameter estimators and their confidence intervals are listed in Table 1. Small dispersion length is assumed: $R = 10^{-4}$. The resulting correlation matrix (not shown here) indicates that there is no strong correlation among the model parameters. The modeling results and experimental data are compared in Fig. 9.

Parameters may also be estimated by the following analysis. f_m be estimated by Eq. (A8) in Appendix, with the available information about the colloids and the porous medium. The next parameter to be estimated is the longitudinal dispersivity/diffusivity. The parameter is relatively low in a homogeneous porous medium, and can be easily fitted to the breakthrough curve.

The estimations of Λ_d and Λ_s are relatively nontrivial. In the case of minimal particle release it is assumed that $\Lambda_r \approx 0$ and $\Lambda_{mr} \approx 0$. The average effluent concentration at the steady state is approximately dependent on $\Lambda_d + \Lambda_s$ alone, since other parameters have little influence on it (see Figs. 5(a), 6(a) and 8(a)). The sum of the two coefficients can approximately be estimated by the logarithm of the average effluent concentration at the steady stage:

$$\Lambda_d + \Lambda_s = -\ln(C_s) \tag{20}$$

where C_s is the average effluent concentration at the steady stage from the experiment. Since the direct deposition from the bulk aqueous phase alone forms the deposited concentration at the inlet, the value of Λ_d can be estimated by fitting the deposition at the inlet. At last, Λ_s is obtained from the estimated value of Λ_d.

The particle velocity is approximated by the average pore water velocity (superficial velocity divided by porosity). The only remaining parameter for estimation is the SA phase deposition rate coefficient Λ_m. It is tuned at last to match the observed position of the deposition maximum.

All the parameters for the calculations are estimated by the above method and shown in Table 2. It can be seen that the esti-

Table 1
Parameter estimators and their confidence intervals (CI) from the proposed model fitting to experiments in Ref. [4].

Experiments	Λ_d	Λ_r	f_m	Λ_s	Λ_m	Λ_{mr}
IS = 3 mM						
Estimator	6.17×10^{-3}	3.74×10^{-4}	0.009993	1.13×10^{-1}	1.32×10^{-1}	2.49×10^{-2}
CI	2.28×10^{-5}	1.77×10^{-6}	2.33×10^{-5}	1.01×10^{-4}	4.58×10^{-4}	6.24×10^{-5}
IS = 6 mM						
Estimator	3.51×10^{-2}	2.71×10^{-4}	0.009999	4.05×10^{-1}	1.35×10^{-1}	2.71×10^{-3}
CI	1.88×10^{-4}	1.62×10^{-6}	1.16×10^{-4}	2.91×10^{-4}	2.18×10^{-3}	2.61×10^{-3}

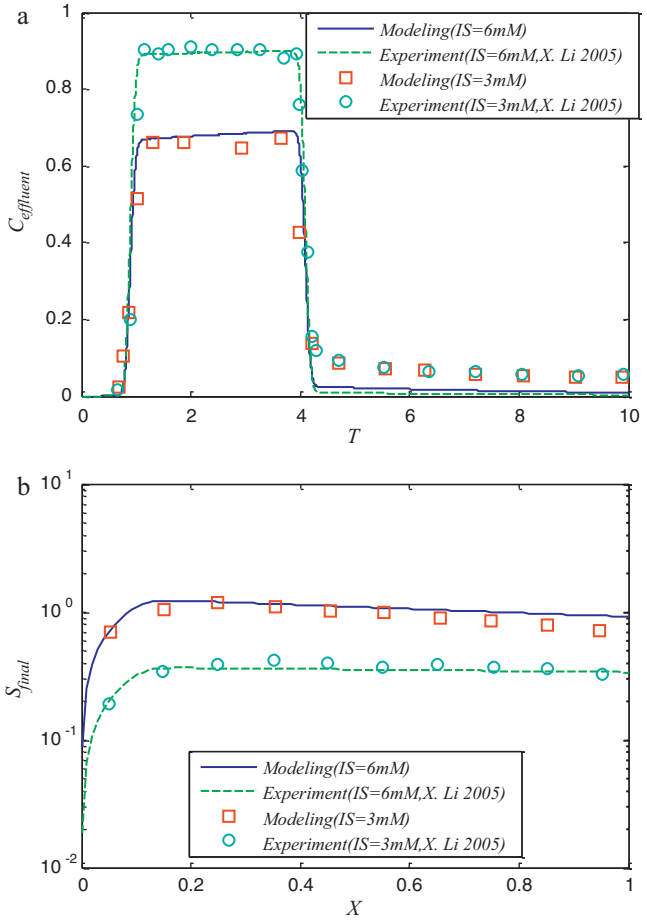

Fig. 9. Results of the proposed model with the parameters estimated by fitting the model to the experiments in Ref. [4].

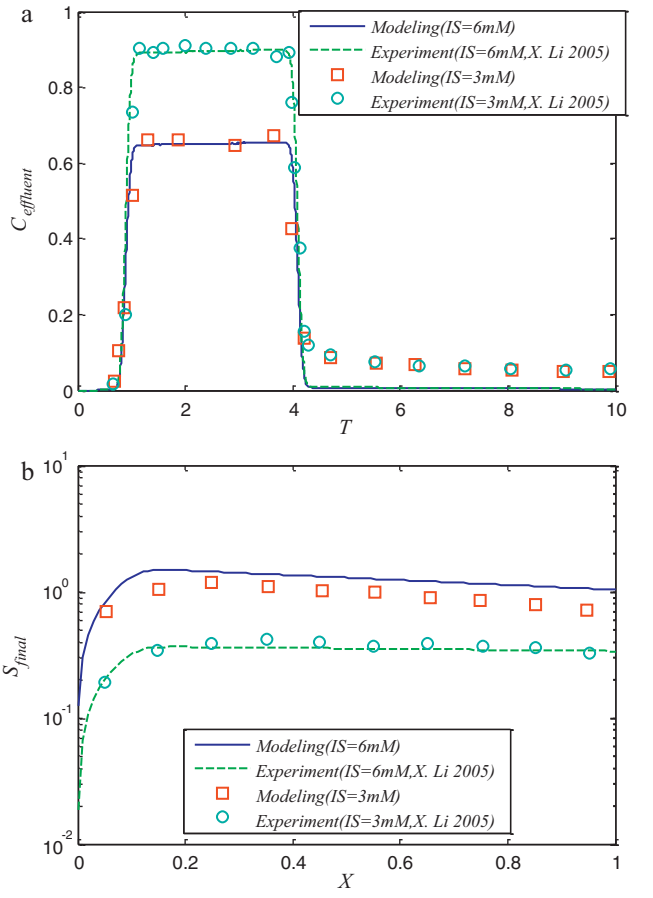

Fig. 10. Results of the proposed model with the parameters estimated by the proposed method and the experimental results in Ref. [4].

mators by fitting the experiments and those by the analysis are close to each other. The modeling results based on the parameters estimated by the above analysis and the experimental data are compared and shown in Fig. 10. In the case of IS = 6 mM the slight overestimation of the deposition can be attributed to neglecting the release of the SA phase and immobilized phase. Both the modeled non-monotonic deposition profile and the breakthrough curve agree with the experimental data. It confirms the ability of the proposed model to simulate a non-monotonic deposition profile in practice and the feasibility of the method for parameter estimation in the case of minimal particle release.

5. Comparison with BSW model

In this section, the proposed model is compared to BSW model from Ref. [18] which can also produce non-monotonic deposition. The purpose is to understand the underlying mechanisms and essence of deposition non-monotonicity by investigating the similarities and differences between the two models.

In Ref. [18], the authors (Bradford, Simunek, and Walker) take into account the release of bacteria aggregates at straining sites. The released aggregates and suspended monodisperse particles are both dispersed in the pore space. The released aggregates are transported and recaptured at different rates from the monodisperse particles. The model in Ref. [18] can be described by the following equations:

$$\frac{\partial C}{\partial T} + u\frac{\partial C}{\partial X} = uR\frac{\partial^2 C}{\partial X^2} - \Lambda_d C \tag{21}$$

$$\frac{\partial C_a}{\partial T} + f_a u\frac{\partial C_a}{\partial X} = f_a uR\frac{\partial^2 C_a}{\partial X^2} - \Lambda_{ad} C_a + F_r S + \Lambda_{ar} S_a \tag{22}$$

$$\frac{\partial S_a}{\partial T} = \Lambda_{ad} C_a - \Lambda_{ar} S_a \tag{23}$$

$$\frac{\partial S}{\partial T} = \Lambda_d C - F_r S \tag{24}$$

$$F_r = \begin{cases} \Lambda_r & S \geq S_c \\ 0 & S < S_c \end{cases} \tag{25}$$

where the subscripts 'a' represent the aggregates, S_c is the critical deposition concentration above which the aggregates start to be released. $\Lambda_d C$ represents the deposition of the suspended monodisperse population at straining sites, $\Lambda_{ad} C_a$ is the deposition rate of the released aggregates and $\Lambda_{ar} S_a$ represents the re-release of the deposited aggregates. f_a reflects the different transport behavior of the aggregates compared to the injected monodisperse particles. Similar boundary conditions as Eqs. (12)–(15) are applied for Eqs. (21) and (22), since there is no aggregate assumed to form before the inlet.

Sample calculations (not shown here) indicate that the transport of aggregates is qualitatively similar to that of the SA phase in our model. The aggregates are generated inside the column domain and

Table 2
Parameters of the proposed model estimated by the proposed method.

Experiments	f_m	Λ_s	Λ_d	Λ_m	Λ_r	Λ_{mr}
IS = 3 mM	0.01	0.108	0.0027	0.135	0	0
IS = 6 mM	0.01	0.405	0.0351	0.135	0	0

Table 3
Parameter estimators and their confidence intervals (CI) from the model in Ref. [18] fitting to experiments in Ref. [4].

Experiments	Λ_d	Λ_r	Λ_{ad}	S_c	Λ_{ar}	f_a
IS = 3 mM						
Estimator	1.19×10^{-1}	3.06×10^{-1}	1.34×10^{1}	1.00×10^{-2}	4.00×10^{-2}	9.90×10^{-1}
CI	8.63×10^{-5}	1.30×10^{-2}	5.81×10^{-1}	2.59×10^{-3}	1.19×10^{-2}	6.59×10^{-2}
IS = 6 mM						
Estimator	3.99×10^{-1}	6.95×10^{-2}	5.35	1.00×10^{-2}	1.11×10^{-10}	9.90×10^{-1}
CI	1.69×10^{-4}	1.64×10^{-4}	1.09×10^{-1}	5.84×10^{-4}	3.57×10^{-12}	1.96×10^{-2}

are transported to the outlet. Unlike the SA phase, the aggregates may contribute much to the breakthrough curve because the velocity of aggregates is comparable to that of the injected monodisperse colloids. The resulting total breakthrough curve may contain two peaks for the monodisperse colloids and the aggregates, respectively. Due to the far slower motion of SA phase, it only has little contribution to the total breakthrough curve.

It can be seen that the two models both consider a third mobile population: surface associated phase via second energy minima and released aggregates, correspondingly. Both additional populations may be transported and immobilized at different rates from the injected population. Neither of them is injected from the inlet. The source of the SA phase is the injected population in the bulk phase, and the source of the aggregates is the accumulated deposition. Mathematically, the two models both involve additional equations for the transport and deposition of the third mobile population. The model structures of them are mathematically similar.

The model in Ref. [18] is also applied to reproduce the experimental results in Ref. [4], as seen in Fig. 11. The modeling results highly agree with the experimental data. The estimated parameters and their confidence intervals are listed in Table 3. A small dispersion length is also assumed: $R = 10^{-4}$. The resulting correlation matrix (not shown here) indicates that there is no strong correlation among the model parameters.

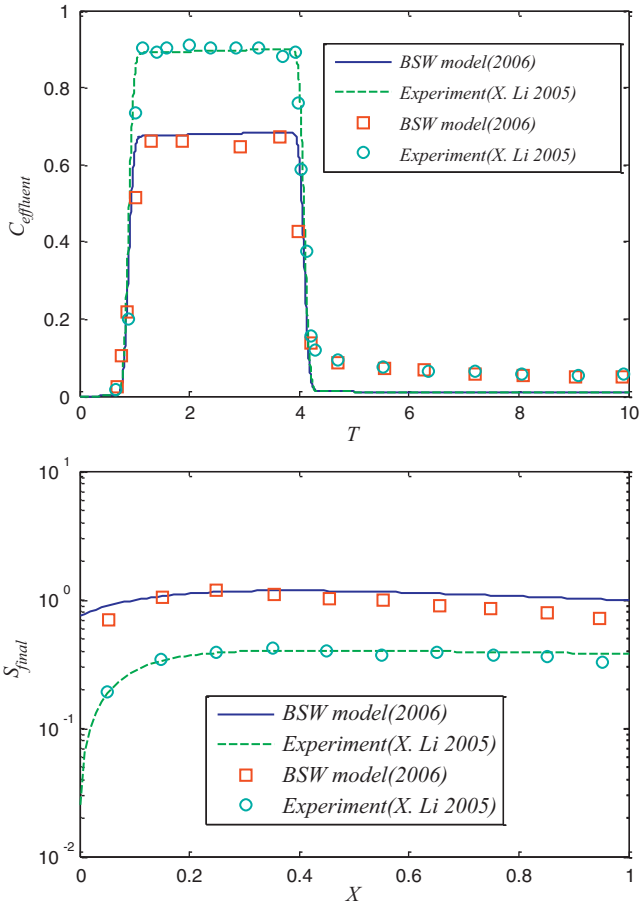

Fig. 11. Results of BSW model [18] with the parameters estimated by fitting the model to the experiments in Ref. [4].

It should be commented that no observation of aggregates has been reported in Ref. [4]. The physics described by the model in Ref. [18] seems to be different from that in these experiments. Nevertheless, the model is still able to reproduce the experimental results. This infers that an additional equation describing a mobile population behaving differently from the injected population seems to be a sufficient condition for producing non-monotonic deposition. The additional equation may reflect different physics in different experimental settings. Selection of a physically correct model requires analysis of the particle behavior on the microscopic scale. Such analysis is not always available and possible. In the last case, in order to match the non-monotonic deposition, the simplest possible model involving the second mobile phase should probably be selected.

6. Conclusions

The proposed model for the suspension/colloid flow in porous media, considering the migration of the surface associated phase, is able to produce non-monotonic deposition profiles. A set of methods for estimating the modeling parameters is provided. The estimation can be easily performed with available experimental information. The results of numerical modeling highly agree with the experimental observations. It confirms the ability of the proposed model to catch a non-monotonic deposition profile in practice and the feasibility of the method for parameter estimation in the case of minimal particle release.

The resulting non-monotonic deposition profiles in Ref. [4] are likely to be caused by the migration of the surface associated phase. An additional equation describing a mobile population behaving differently from the injected population seems to be a sufficient condition for producing non-monotonic deposition profiles.

Acknowledgement

This work is funded by the Danish Council for Independent Research, Technology and Production Sciences (FTP), which is kindly acknowledged for financial support.

Appendix A. Appendix

A.1. Magnitude of SA phase migration

The appendix presents a rough estimation method for the magnitude of f_m. Since packed beds of granular media are commonly adopted in filtration experiments, they are also selected for the study here. The type of media can be represented by various geometrical models [42,47–50]. The constricted tube model [26,42] is applied in this work. The grains of the porous medium and the colloid particles are assumed to be spherical. It may also be assumed

that the velocity of a particle adjacent to the pore wall via the second energy minimum may be approximated by the fluid velocity at its center. In Ref. [26] the diameter of the pore in a different position z can be expressed as:

$$d_z = 2\left\{\frac{d_{\max}}{2} + \left[4\left(\frac{d_c}{2} - \frac{d_{\max}}{2}\right)\left(0.5 - \frac{z}{h}\right)^2\right]\right\}, \quad \text{(A1)}$$

where $d_{\max}$ is the maximum diameter of the pore, d_c is the constriction diameter, and h is the pore length. In Ref. [42] d_c and the effective pore diameter $d_{effective}$ are calculated by:

$$d_c = \frac{d_{media}}{2.5658}, \quad \text{(A2)}$$

$$d_{effective} = \frac{d_c}{0.47}, \quad \text{(A3)}$$

where d_{media} is the diameter of the bed median particle, and in Ref. [47] $d_{\max}$ is calculated by:

$$d_{\max} = 2.141 d_c. \quad \text{(A4)}$$

In Ref. [26] the fluid velocity is then calculated by:

$$v_{colloid} = 2\frac{Q/N_{pore}}{(\pi/4))d_z^2}\left[1 - \frac{d_z - d_{colloid}}{d_z}\right] \quad \text{(A5)}$$

where $d_{colloid}$ is the diameter of the colloid particle, Q is the volumetric flow rate, d_z is the pore diameter in the position z, and N_{pore} is the number of pores in a cross-section of the column, which can be expressed as:

$$N_{pore} = \frac{A\varphi}{(\pi/4)d_{effective}^2} \quad \text{(A6)}$$

where A is the cross-section area of the column, φ is the porosity of the column. The fraction f_m can be approximated by the velocity across the center of the associated particle divided by the average pore velocity:

$$f_m = \frac{v_{colloid}}{Q/A\phi} = \frac{2d_{effective}^2 d_{colloid}}{d_z^3} \quad \text{(A7)}$$

With given media particle size and the suspended or colloid particle size, the fraction fm is a function of z/h. Sample calculations are performed for the experimental setting in [4], plots of f_m to z/h are shown in Fig. 12(a). It is seen that the fraction approaches its maximum at the inlet and the outlet of the pore. The average of the fraction f_m can be calculated by:

$$f_m \approx \overline{f_m} = \frac{\int_0^1 f_m d(z/h)}{\int_0^1 d(z/h)} = \int_0^1 f_m d(z/h)$$
$$f_m = \frac{d_{colloid}}{d_{media}}\int_0^1 \frac{1.3748}{8[0.4172 - 0.8892(0.5 - (z/h))^2]^3} d(z/h) \quad \text{(A8)}$$
$$f_m = 5.7396\frac{d_{colloid}}{d_{media}}$$

The plot of average f_m versus typical suspended/colloid particle sizes and typical median particle sizes is shown in Fig. 12(b). It is seen that the typical value of f_m varies approximately from 1×10^{-2} to 5×10^{-2}.

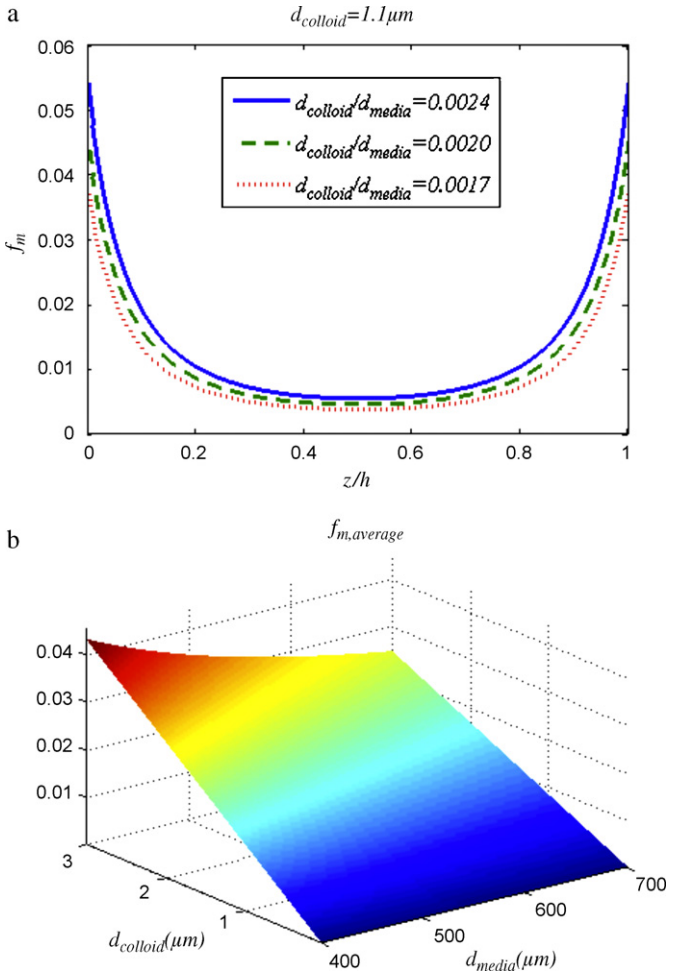

Fig. 12. (a) f_m at different pore positions, (b) average f_m for different diameters of colloids and those of median particles.

References

[1] M. Elimelech, J. Gregory, R. Williams, X. Jia, Particle Deposition & Aggregation: Measurement, Modelling and Simulation (Colloid & Surface Engineering), Butterworth-Heinemann, 1998.
[2] F. Civan, Reservoir Formation Damage, Gulf Professional Publishing, USA, 2000.
[3] J.P. Herzig, D.M. Leclerc, P.L. Goff, Flow of suspensions through porous media-application to deep filtration, Industrial & Engineering Chemistry 62 (1970) 8–35.
[4] X. Li, W.P. Johnson, Nonmonotonic variations in deposition rate coefficients of microspheres in porous media under unfavorable deposition conditions, Environmental Science & Technology 39 (2005) 1658–1665.
[5] A. Cortis, B. Berkowitz, Anomalous Transport in "Classical" Soil and Sand Columns, Soil Science Society of America Journal 68 (2004) 1539–1548.
[6] M. Fourar, G. Radilla, Non-Fickian description of tracer transport through heterogeneous porous media, Transport in Porous Media 80 (2009) 561–579.
[7] M. Levy, B. Berkowitz, Measurement and analysis of non-Fickian dispersion in heterogeneous porous media, Journal of Contaminant Hydrology 64 (2003) 203–226.
[8] X. Li, P. Zhang, C.L. Lin, W.P. Johnson, Role of hydrodynamic drag on microsphere deposition and re-entrainment in porous media under unfavorable conditions, Environmental Science & Technology 39 (2005) 4012–4020.
[9] S.A. Bradford, M. Bettahar, J. Simunek, M.T.v. Genuchten, Straining and attachment of colloids in physically heterogeneous porous media, Vadose Zone Journal 3 (2004) 384–394.
[10] J.A. Redman, S.L. Walker, M. Elimelech, Bacterial adhesion and transport in porous media: role of the secondary energy minimum, Environmental Science & Technology 38 (2004) 1777–1785.
[11] N. Tufenkji, M. Elimelech, Deviation from the classical colloid filtration theory in the presence of repulsive DLVO interactions, Langmuir 20 (2004) 10818–10828.
[12] N. Tufenkji, J.A. Redman, M. Elimelech, Interpreting deposition patterns of microbial particles in laboratory-scale column experiments, Environmental Science & Technology 37 (2003) 616–623.
[13] J.A. Redman, M.K. Estes, S.B. Grant, Resolving macroscale and microscale heterogeneity in virus filtration, Colloids and Surfaces A: Physicochemical and Engineering Aspects 191 (2001) 57–70.
[14] N. Tufenkji, M. Elimelech, Breakdown of colloid filtration theory: role of the secondary energy minimum and surface charge heterogeneities, Langmuir 21 (2005) 841–852.
[15] X. Li, C.L. Lin, J.D. Miller, W.P. Johnson, Pore-scale observation of microsphere deposition at grain-to-grain contacts over assemblage-scale porous media

domains using X-ray microtomography, Environmental Science & Technology 40 (2006) 3762–3768.
[16] X. Li, C.L. Lin, J.D. Miller, W.P. Johnson, Role of grain-to-grain contacts on profiles of retained colloids in porous media in the presence of an energy barrier to deposition, Environmental Science & Technology 40 (2006) 3769–3774.
[17] S.A. Bradford, S. Torkzaban, F. Leij, J. im, M.T. nek, van Genuchten, Modeling the coupled effects of pore space geometry and velocity on colloid transport and retention, Water Resources Research 45 (2009) W02414.
[18] S.A. Bradford, J. Simunek, S.L. Walker, Transport and straining of *E. coli* O157:H7 in saturated porous media, Water Resources Research 42 (2006), W12S12.
[19] P. Bedrikovetsky, F. Siqueira, C. Furtado, A. Souza, Modified particle detachment model for colloidal transport in porous media, Transport in Porous Media (2010) 1–31.
[20] S.A. Bradford, S. Torkzaban, S.L. Walker, Coupling of physical and chemical mechanisms of colloid straining in saturated porous media, Water Research 41 (2007) 3012–3024.
[21] M. Elimelech, C.R. O'Melia, Kinetics of deposition of colloidal particles in porous media, Environmental Science & Technology 24 (1990) 1528–1536.
[22] S.A. Bradford, J. Simunek, M. Bettahar, M.T. Van Genuchten, S.R. Yates, Modeling colloid attachment, straining, and exclusion in saturated porous media, Environmental Science & Technology 37 (2003) 2242–2250.
[23] S.A. Bradford, J. Simunek, M. Bettahar, M.T. van Genuchten, S.R. Yates, Significance of straining in colloid deposition: evidence and implications, Water Resources Research 42 (2006) W12S15.
[24] S.A. Bradford, M. Bettahar, Straining, attachment, and detachment of cryptosporidium oocysts in saturated porous media, Journal of Environmental Quality 34 (2005) 469–478.
[25] M. Tong, X. Li, C.N. Brow, W.P. Johnson, Detachment-influenced transport of an adhesion-deficient bacterial strain within water-reactive porous media, Environmental Science & Technology 39 (2005) 2500–2508.
[26] J. Bergendahl, D. Grasso, Prediction of colloid detachment in a model porous media: hydrodynamics, Chemical Engineering Science 55 (2000) 1523–1532.
[27] W.P. Johnson, X. Li, S. Assemi, Deposition and re-entrainment dynamics of microbes and non-biological colloids during non-perturbed transport in porous media in the presence of an energy barrier to deposition, Advances in Water Resources 30 (2007) 1432–1454.
[28] S. Torkzaban, S.A. Bradford, S.L. Walker, Resolving the coupled effects of hydrodynamics and DLVO forces on colloid attachment in porous media, Langmuir 23 (2007) 9652–9660.
[29] S. Torkzaban, S.S. Tazehkand, S.L. Walker, S.A. Bradford, Transport and fate of bacteria in porous media: coupled effects of chemical conditions and pore space geometry, Water Resources Research 44 (2008) W04403.
[30] C.N. Brow, X. Li, J. Ricka, W.P. Johnson, Comparison of microsphere deposition in porous media versus simple shear systems, Colloids and Surfaces A: Physicochemical and Engineering Aspects 253 (2005) 125–136.
[31] S.L. Walker, J.A. Redman, M. Elimelech, Role of cell surface lipopolysaccharides in *Escherichia coli* K12 adhesion and transport, Langmuir 20 (2004) 7736–7746.
[32] W.P. Johnson, M. Tong, Observed and simulated fluid drag effects on colloid deposition in the presence of an energy barrier in an impinging jet system, Environmental Science & Technology 40 (2006) 5015–5021.
[33] W.P. Johnson, X. Li, G. Yal, Colloid retention in porous media: mechanistic confirmation of wedging and retention in zones of flow stagnation, Environmental Science & Technology 41 (2007) 1279–1287.
[34] X. Li, T.D. Scheibe, W.P. Johnson, Apparent decreases in colloid deposition rate coefficients with distance of transport under unfavorable deposition conditions: a general phenomenon, Environmental Science & Technology 38 (2004) 5616–5625.
[35] S.A. Bradford, N. Toride, A stochastic model for colloid transport and deposition, Journal of Environmental Quality 36 (2007) 1346–1356.
[36] H. Yuan, A.A. Shapiro, Modeling non-Fickian transport and hyperexponential deposition for deep bed filtration, Chemical Engineering Journal 162 (2010) 974–988.
[37] F.J. Leij, S.A. Bradford, Combined physical and chemical nonequilibrium transport model: analytical solution, moments, and application to colloids, Journal of Contaminant Hydrology 110 (2009) 87–99.
[38] A.A. Shapiro, P.G. Bedrikovetsky, A stochastic theory for deep bed filtration accounting for dispersion and size distributions, Physica A: Statistical Mechanics and its Applications 389 (2010) 2473–2494.
[39] M.T. Van Genuchten, Analytical solutions for chemical transport with simultaneous adsorption, zero-order production and first-order decay, Journal of Hydrology 49 (1981) 213–233.
[40] M. Omlin, P. Reichert, A comparison of techniques for the estimation of model prediction uncertainty, Ecological Modelling 115 (1999) 45–59.
[41] D.M. Bates, D.G. Watts, Nonlinear Regression Analysis & Applns P, Wiley-Interscience, USA, 2003.
[42] S.K. Chan, K.M. Ng, Geometrical characteristics of the pore space in a random packing of equal spheres, Powder Technology 54 (1988) 147–155.
[43] M.J. Blunt, Flow in porous media—pore-network models and multiphase flow, Current Opinion in Colloid & Interface Science 6 (2001) 197–207.
[44] K.E. Thompson, H.S. Fogler, Modeling flow in disordered packed beds from pore-scale fluid mechanics, AIChE Journal 43 (1997) 1377–1389.
[45] C. Pan, M. Hilpert, C.T. Miller, Pore-scale modeling of saturated permeabilities in random sphere packings, Physical Review E 64 (2001) 066702.
[46] Y. Zhu, P.J. Fox, J.P. Morris, A pore-scale numerical model for flow through porous media, International Journal for Numerical and Analytical Methods in Geomechanics 23 (1999) 881–904.
[47] A.C. Payatakes, A new model for granular porous media. Part I: Model formulation, American Institue of Chemical Engineers Journal 19 (1973) 58–66.
[48] A.C. Payatakes, R. Rajagopalan, C. Tien, Application of porous media models to the study of deep bed filtration, The Canadian Journal of Chemical Engineering 52 (1974) 722–731.
[49] A.C. Payatakes, C. Tien, R.M. Turian, Trajectory calculation of particle deposition in deep bed filtration. Part I: Model formulation, AIChE Journal 20 (1974) 889–900.
[50] C. Tien, B.V. Ramarao, Granular Filtration of Aerosols and Hydrosols, Second edition, Elsevier Science, Oxford, 2007.